Rare Metal Materials and Engineering
Volume 55, Issue 5, May 2026
Available online at www.rmme.ac.cn

Science Press

Cite this article as: Song Zhuo, Li Huanqing, Tian Xiaolin, et al. Designing Optimal Temperature for Multi-directional Forging Process: A Phase-Field Crystal Study[J]. Rare Metal Materials and Engineering, 2026, 55(05): 1146-1156. DOI: https://doi.org/10.12442/j.issn.1002-185X.20250354.

ARTICLE

Designing Optimal Temperature for Multi-directional Forging Process: A Phase-Field Crystal Study

Song Zhuo[1], Li Huanqing[1], Tian Xiaolin[1], Kang Xiaolan[1], Hou Hua[1,4], Zhao Yuhong[1,2,3]

[1] Shanxi Key Laboratory of Intelligent Casting and Advanced Forming for New Materials, Collaborative Innovation Center for Research and Application of Aluminum/Magnesium Materials, School of Materials Science and Engineering, North University of China, Taiyuan 030051, China; [2] Beijing Advanced Innovation Center for Materials Genome Engineering, University of Science and Technology Beijing, Beijing 100083, China; [3] Institute of Materials Intelligent Technology, Liaoning Academy of Materials, Shenyang 110004, China; [4] School of Materials Science and Engineering, Taiyuan University of Science and Technology, Taiyuan 030024, China

Abstract: Using multi-directional forging temperature as the independent variable and adopting the dual-mode phase field crystal model, the nucleation modes, reaction mechanisms, and interactions between grain boundaries and dislocations at different temperatures were investigated. Results show that a mapping relationship between process parameters and grain refinement/coarsening is established, and the optimal processing temperature coefficient is 0.23. Compared with the cases with processing temperature coefficient of 0.19, 0.20, 0.21, 0.25, and 0.27, the refinement effect increases by 256.0%, 146.0%, 113.0%, 6.7%, and 52.4%, respectively. Excessively high temperatures lead to grain coarsening due to dislocation annihilation, and the application of strain can reduce the actual melting point of materials. Even if the processing temperature does not exceed the theoretical melting point, remelting and crystallization may still occur, resulting in an overburning phenomenon that reduces internal defects and increases overall grain size. This research is of great significance for the actual forging process design.

Key words: phase-field crystal method; multi-directional forging; temperature; grain refinement; dislocation

1 Introduction

The multi-directional forging process was proposed in the 1990s. Multi-directional forging[1], hot extrusion[2], high-pressure torsion[3], and equal-channel angular pressing[4] are widely employed techniques in the plastic deformation processing of materials. The principle of the process is to perform multi-pass high-temperature compression on materials along different directions by the forging equipment, therefore refining the grains by dynamic recrystallization during the deformation process. Multi-directional forging process parameters have a significant effect on product performance. The main influencing factors are cumulative strain, strain rate, processing temperature, initial grain structure, lubricant, and heat treatment process after forging[5–6]. Yang et al[7] reported that the lower temperature reduces atomic motion and decreases the mobility of grain boundaries, thereby inhibiting the grain growth. Conversely, high temperatures diminish the bending stiffness and integrity of thinned grains, facilitating the formation of band structures, which in turn promotes recrystallization. Rao et al[5] found that more equiaxed subgrains can be produced by cryogenic multi-directional forging. Huang et al[8] investigated the Ti-6Al-4V alloy and found that the average grain size is increased with the increase in initial forging temperature. However, the specific mechanisms underlying grain boundary migration and the principles governing dislocation density variations at different forging temperatures require further investigation.

It is found that the temperature has a great influence on the multi-directional forging results. At present, the research on the multi-directional forging process is mainly based on

Received date: July 03, 2025
Foundation item: National Natural Science Foundation of China (52375394, 52275390, U23A20628, 52305429); Major Project of Science and Technology in Shanxi (202301050201004); Natural Science Foundation of Shanxi Province (202403021222132)
Corresponding author: Zhao Yuhong, Ph. D., Professor, Shanxi Key Laboratory of Intelligent Casting and Advanced Forming for New Materials, Collaborative Innovation Center for Research and Application of Aluminum/Magnesium Materials, School of Materials Science and Engineering, North University of China, Taiyuan 030051, P. R. China, E-mail: zhaoyuhong@nuc.edu.cn

experiments. However, the mechanisms underlying nanoscale grain boundary migration and dislocation formation remain inadequately explained. Furthermore, with the increasingly complex, diversified, and harsh material application environment, the research on the interactions between traditional laboratory environments and materials is insufficient. With the advent of the information age, computer simulation technology has been applied to many fields. Currently, it can conduct a comprehensive and in-depth study of materials from nanoscale microstructure to macroscopic morphology[9–12]. In the realm of computational simulation, phase-field method (PFM) has emerged as a predominant approach to predict the evolution of nanoscale and mesoscopic microstructures and their properties during material processing[13–18]. It effectively bridges the gap between atomic-scale methods and macroscale applications[19–21]. PFM plays an important role in understanding and explaining experimental phenomena and reducing experimental costs[22–25].

Elder et al[26] proposed the phase-field crystal (PFC) method in 2002. The significant advantage of this method is that it combines the atomic length scale and the diffusion time scale, and it can self-consistently consider the generation of structural defects, such as dislocations and grain boundaries, and the evolution of defects and phase morphology under the action of elasticity. At present, PFC method has been widely used to study grain nucleation and growth[27], recrystallization[28], phase transformation[29], crack propagation[30–31], grain boundary pre-melting[32], and nanograin boundaries and twins[33–35]. Additionally, PFC method can also realize the microscopic explanation of the internal mechanism of the whole process of casting→heat treatment→deformation process→defect prediction[36–39] to assist the design and development of new materials.

In this research, PFC module in EPhase (a phase field software independently developed by Professor Zhao Yuhong's team) was used to explore the influence of different temperature parameters on the grain refinement effect of multi-directional forging and the detailed mechanism of grain refinement. The investigation on grain refinement, coarsening mechanism, and dislocation nucleation mechanism in the multi-directional forging process, as well as the influence of forging temperature on the grain refinement effect, provided theoretical support and guidance for parameter selection and optimization in the actual production process.

2 Model and Parameter Settings

2.1 PFC model

In this research, the influence of temperature on the results of multi-directional forging was investigated using a two-mode PFC model. The temperature coefficient ϵ used in the simulation is a dimensionless representation of temperature in the actual experiment. It can be expressed as a function of temperature, $\epsilon = \alpha\Delta T/\lambda q_0^4$, and it is used to non-dimensionalize the temperature.

The dimensionless free energy functional F can be expressed as follows:

$$F = \int\left(\frac{\psi}{2}\left\{-\epsilon + \left(1+\nabla^2\right)^2\left[R_1 + \left(\nabla^2 + Q_1^2\right)^2\right]\right\}\psi + \frac{1}{4}\psi^4\right)\mathrm{d}\boldsymbol{r} \quad (1)$$

where $\boldsymbol{r}$ represents the position vector of the atoms; ψ is the periodic local atomic density; ϵ is the temperature-related parameter; ∇^2 is the Laplace operator; R_1 is related to the relative stability of different crystal structures with R_1=1 in this research; $Q_1 = \sqrt{2}$ and its value is generally determined by the choice of crystal structure. Q_1 can be obtained by the ratio of the module of the second-nearest neighbor reciprocal lattice vector to the module of the nearest neighbor reciprocal lattice vector.

The dimensionless dynamic equation is as follows:

$$\frac{\partial\psi}{\partial t} = \nabla^2\frac{\partial F}{\partial\psi} = \nabla^2\left[-\epsilon\psi + \left(\nabla^2+1\right)^2\left(\nabla^2+2\right)^2\psi + \psi^3\right] \quad (2)$$

where t is the time variable.

The semi-implicit Fourier spectral method is used in this research. Therefore, Eq.(2) can be expressed in Fourier space, as follows:

$$\psi_{\boldsymbol{k},t+1} = \frac{\psi_{\boldsymbol{k},t} - \boldsymbol{k}^2\Delta t\psi_{\boldsymbol{k},t}^3}{1 + \boldsymbol{k}^2\Delta t\left[\left(4-\epsilon\right) - 12\boldsymbol{k}^2 + 13\boldsymbol{k}^4 - 6\boldsymbol{k}^6 + \boldsymbol{k}^8\right]} \quad (3)$$

where $\psi_{\boldsymbol{k}}$ represents a Fourier transform; $\boldsymbol{k}$ represents a Fourier space vector and satisfies the $\boldsymbol{k}^2 = |\boldsymbol{k}|^2$.

The grain will deform under the strain loading of multi-directional forging. Uniaxial tensile loading and equal area deformation were adopted in the simulation, and the tensile direction was opposite to the actual forging loading direction. Therefore, the y-axis stretching in the simulation represents the x-axis compression in the actual forging loading. In the same area condition, the space step in the x direction was assumed to have an increment $d = \dot{\varepsilon}\Delta x\Delta t$ at each step, where $\dot{\varepsilon} = 6\times10^{-5}/\Delta t$ is the dimensionless strain rate. Therefore, it is assumed that there is an equal area condition, as follows:

$$S = \Delta x\times\Delta y = \Delta x'\times\Delta y' \quad (4)$$

where Δx and Δy represent the grid sizes before deformation along x-axis and y-axis, respectively; $\Delta x'$ and $\Delta y'$ represent the grid sizes after deformation along x-axis and y-axis, respectively. The space step sizes in the x and y directions after stretching along the y-axis are expressed by Eq.(5–6), respectively:

$$\Delta x' = \Delta x\times\Delta y/\Delta y' = \Delta x/\left(1+n\dot{\varepsilon}\Delta t\right) \quad (5)$$

$$\Delta y' = \Delta y + nd = \Delta y + n\dot{\varepsilon}\Delta y\Delta t = \Delta y\left(1+n\dot{\varepsilon}\Delta t\right) \quad (6)$$

By the same token, the spatial step sizes of the x and y directions after stretching and deformation of the x-axis can also be obtained, as follows:

$$\Delta x' = \Delta x + nd = \Delta x + n\dot{\varepsilon}\Delta x\Delta t = \Delta x\left(1+n\dot{\varepsilon}\Delta t\right) \quad (7)$$

$$\Delta y' = \Delta x\times\Delta y/\Delta x' = \Delta y/\left(1+n\dot{\varepsilon}\Delta t\right) \quad (8)$$

It is possible to relate the forging process of the actual three-dimensional material through isovolumetric deformation with the specific relationship equation $\Delta x = \Delta y = \left|1-\sqrt{1/\left(1-\Delta z\right)}\right|$, where Δx and Δy are the deformations of the studied two-dimensional sections, and Δz is the deformation of the z-axis in three dimensions under applied strain. The relationship

among the actual loading strain E, the strain rate $\dot{\varepsilon}$, the number of steps n, and the time step Δt in the simulation is $E = n\dot{\varepsilon}\Delta t$.

2.2 Parameter settings

To reduce the calculation time, the simulation area was set to as $L_x \times L_y = 512\Delta x \times 512\Delta y$. The time step $\Delta t = 0.5$, and the space step $\Delta x = \Delta y = \pi/4$. At the same time, the optimal loading parameters in Ref. [40] (three-pass loading: $t^*_{Y1}=1500$, $t^*_{X1}=1500$, and $t^*_{Y2}=1000$, where t^*_{Y1}, t^*_{X1}, and t^*_{Y2} represent the time in the simulation with subscripts $Y1$, $X1$, and $Y2$ representing the direction of the first/second loading stress on the X and Y axes; strain rate $\dot{\varepsilon} = 6 \times 10^{-5}/\Delta t$). According to the thermodynamic phase diagram, different temperature coefficients are selected, as shown in Fig. 1. Six different processing temperature schemes were adopted in this research, and the specific parameters are shown in Table 1. Four groups of typical results with the temperature coefficient ϵ_1 of 0.27, 0.21, 0.20, and 0.19 were analyzed in detail.

In this research, the orientation angles of Grain 1 (G1), Grain 2 (G2), twin grain 1 (TG1), and twin grain 2 (TG2) were set as $th_{G1} = -10°$, $th_{G2} = 5°$, $th_{TG1} = 20°$, and $th_{TG2} = -20°$, respectively. Certain regions were left between the nuclei as liquid phase regions, as shown in Fig. 2a. In the process of grain growth, the nucleus is gradually merged with the surrounding liquid phase and eventually forms a grain boundary (GB) at the pairwise junction (Fig.2b). GB-2, GB-3, GB-5, and GB-6 in Fig.2b are defined as horizontal GBs, and GB-1 and twin boundaries (TBs, GB-4 and GB-7) are defined as vertical GBs.

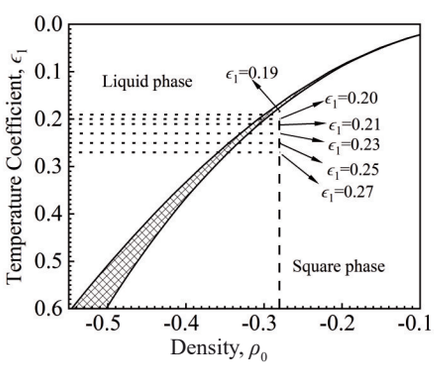

Fig.1 Two-mode thermodynamic phase diagram

Table 1 Processing parameters

Scheme	Temperature coefficient of multi-directional forging, ϵ_1
1	0.27
2	0.25
3	0.23
4	0.21
5	0.20
6	0.19

3 Simulation Results

3.1 Analysis with temperature coefficient ϵ_1=0.27

Fig. 3 shows the density field evolution results when the temperature coefficient is 0.27, and GB bends when t^*=1500. The tip of stress concentration is formed at the curved GB, as shown in the red dotted area in Fig.3a. Subsequently, the two-pass loading stage starts. At the end of this stage, the dislocations at TBs merge into the grains, as shown in the yellow dotted areas in Fig. 3b – 3c. At the beginning of the three-pass loading, due to the change in the loading direction, the dislocations separated from TBs move to TB area and re-enter TBs, so the TB structure changes, as shown in Fig. 3d–3e. The area surrounded by yellow atoms in Fig. 3e is part of TB with a complex structure.

When t^* =3300 (in the three-pass loading stage), the dislocations from GB-3 enter into Grain 2, and a large number of dislocations from GB-4 enter into the twin grains on both sides. The path formed by GB-4 and the induced dislocation movement jointly lead to a branch shape, and new dislocations are formed in the middle and end parts of the branch. At the same time, GB-1 bends under stress to form a tip of stress concentration, as shown in Fig. 3f – 3g. With the continuous loading of stress, the dislocations from the tip of GB-1 area enter into Grain 1 and Grain 2 on both sides, so the concentrated stress is released, and GB-1 turns into a relatively smooth state. At the same time, a group of dislocations in Grain 4 move under stress, and a relatively obvious annihilation reaction occurs in Grain 4, as shown in Fig. 3h – 3i. The nucleation and subsequent motion of dislocations jointly lead to fragment of initial grains. This

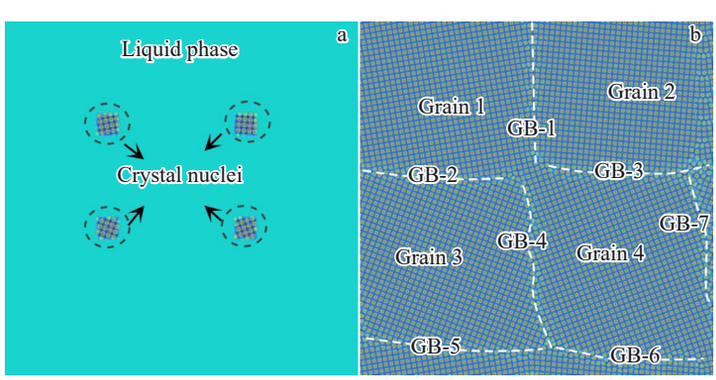

Fig.2 Schematic diagrams of initial grain setting (a) and grain solidification growth (b)

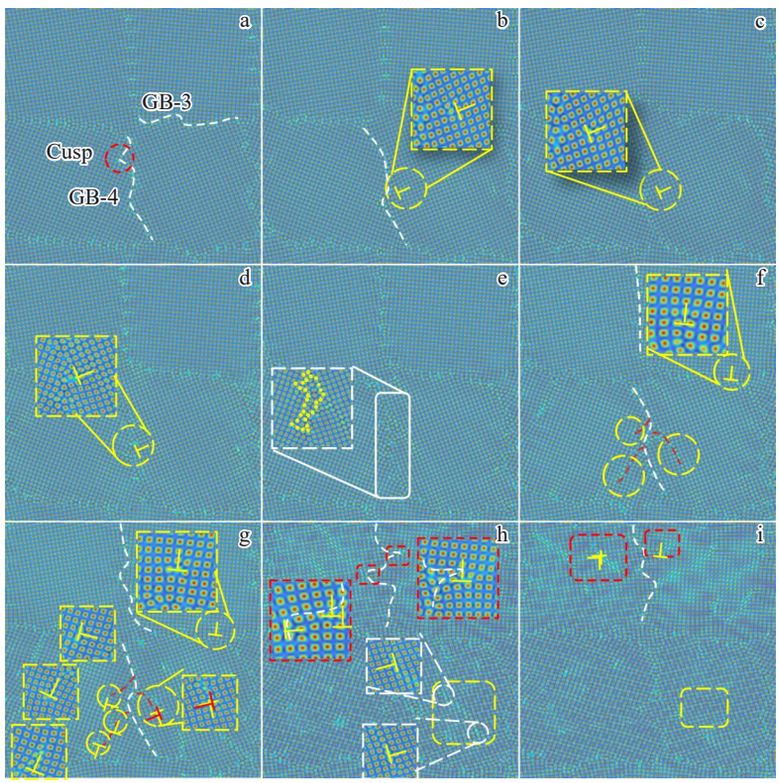

Fig.3 Density field evolution results of multi-directional forging with temperature coefficient ϵ_1=0.27 during one-pass (a), two-passes (b–c), and three-passes (d–i) loading stages: (a) t^*=1500; (b) t^*=1600; (c) t^*=3000; (d) t^*=3100; (e) t^*=3200; (f) t^*=3300; (g) t^*=3500; (h) t^*=3900; (i) t^*=4000

process ultimately results in grain refinement.

3.2 Analysis with temperature coefficient ϵ_1=0.21

When the temperature coefficient rises to 0.21, the overall trend of microstructure evolution in the first two stages does not change. When t^*=3000, no dislocations from GB-3 and GB-4 enter into the grain interior, as indicated by the white dotted lines in Fig. 4b. At the initial moment of the three-passes loading stage, the atoms in some areas near TB are misaligned under stress. At the same time, because the temperature is close to the solidus line temperature, the atoms in TB region are transformed into disordered ones under the dual action of stress and high temperature, as shown in Fig. 4c. With the continuous loading of stress, new dislocations are generated in the atomic misaligned region, and TB atoms change from disordered ones to ordered atoms again, as shown in Fig.4d.

When t^*=3400, some dislocations from GBs in Grain 1 and Grain 2 encounter with each other and disappear under the stress, as shown in the yellow dotted areas in Fig. 4e–4g. A disc-like structure composed of vacancies is formed in TBs, and the disc-like structure causes serious lattice distortion, as shown in the red dotted regions of Grain 3 in Fig. 4g. At the same time, a large number of dislocations in twin grains disappear, as shown in Fig. 4g–4i. The defect structure in the white dotted area inside Grain 3 is taken as the object. When t^*=3600, the number of dislocations is 7, and there are two disk-like structures. When t^*=3800, the number of dislocations is 8, the disk-like structure disappears, and the total number of defects decreases. When t^*=4000, it is found that the defect structure disappears more obviously, the number of dislocations is 5, and a two-atom-sized disk-like structure is found.

Therefore, when the processing temperature coefficient rises to 0.21, the grains are coarsened at high temperatures, and the grain refinement effect induced by multi-directional forging is also degraded.

3.3 Analysis with temperature coefficient ϵ_1=0.20

When the temperature coefficient changes to 0.20, the simulation results are shown in Fig. 5. In the stage of t^*=1–3000, the overall evolution trend of the microstructure with temperature coefficient of 0.20 is similar to that of 0.21. At t^*=3100, the atoms in some areas near TB are misaligned under stress. At the same time, the temperature is closer to the solidus line temperature, and the atoms in most areas of TB are under the dual action of stress and high temperature, resulting in a more obvious transition from ordered atoms to disordered ones, as shown in Fig.5c.

When t^*=3300, part of the dislocations from GB entering into the interior of Grain 1 and Grain 2 begin to move under stress. Then, they encounter with each other and eventually disappear in the grains. This phenomenon is the same as that when ϵ_1 is 0.21, as shown in the yellow doted areas in Fig. 5d–5f. At the same time, a disc-like structure is generated inside the grain, which migrates under stress and eventually collapses near GB to form an atomic staggered structure.

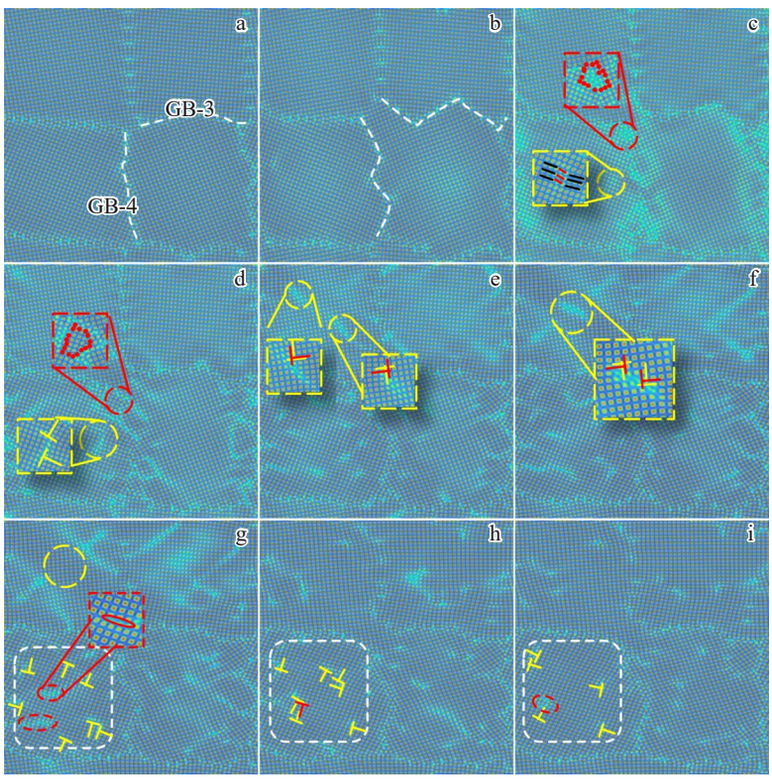

Fig.4 Density field evolution results of multi-directional forging with temperature coefficient ϵ_1=0.21 during one-pass (a), two-passes (b), and three-passes (c–i) loading stages: (a) t^*=1500; (b) t^*=3000; (c) t^*=3100; (d) t^*=3200; (e) t^*=3400; (f) t^*=3500; (g) t^*=3600; (h) t^*=3800; (i) t^*=4000

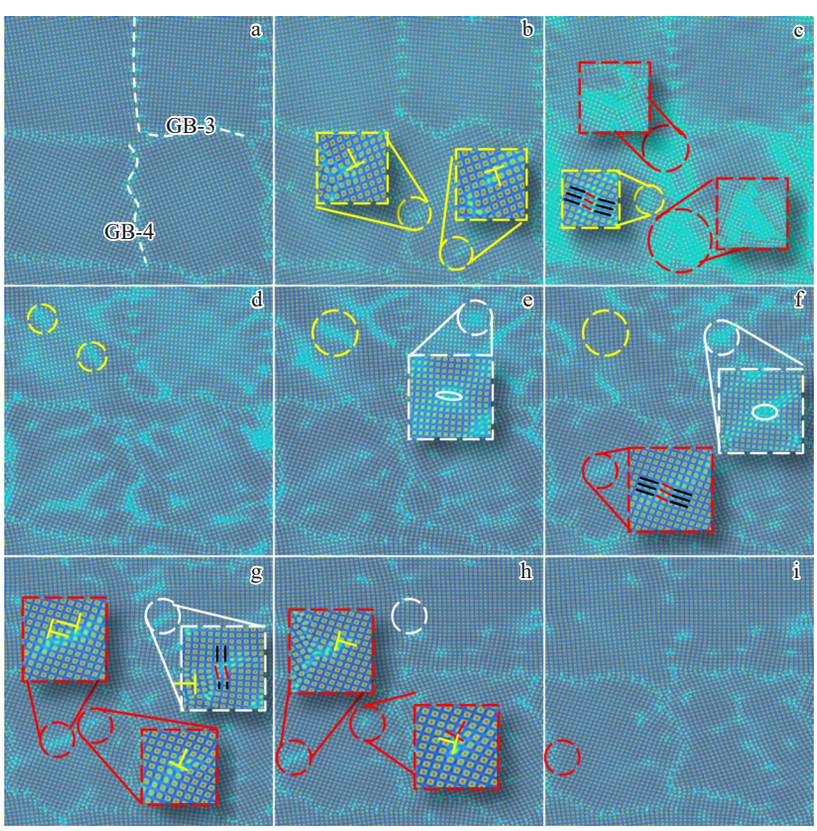

Fig.5 Density field evolution results of multi-directional forging with temperature coefficient ϵ_1=0.20 during one-pass (a), two-passes (b), and three-passes (c–i) loading stages: (a) t^*=1500; (b) t^*=2900; (c) t^*=3100; (d) t^*=3300; (e) t^*=3400; (f) t^*=3500; (g) t^*=3600; (h) t^*=3800; (i) t^*=4000

Subsequently, the staggered area reacts with GB and eventually disappears, as shown in Fig. 5e – 5h. The twin crystal Grain 3 firstly forms the atomic dislocation under stress, and then the dislocation nucleation occurs in the dislocation region. The dislocation after nucleation moves to the left and right sides of GB under stress. Finally, some dislocations enter into the left part of GB, and some dislocations move below the dislocation marked by red dotted area, as shown in Fig. 5f – 5i. Through the abovementioned mechanism, the number of dislocations in the whole region is finally reduced, and the grains are coarsened.

3.4 Analysis with temperature coefficient ϵ_1=0.19

When the temperature coefficient changes to 0.19, the simulation results are shown in Fig. 6. In the stage of t^*=1 – 3000, the overall evolution trend of the microstructure with temperature coefficient of 0.19 is similar to that of 0.20. When t^*=3000, some areas of GB-1 form a disk-like structure, as shown in the red dotted area in Fig. 6c. During the three-passes stage, a large area of remelting occurs from TB to the outward diffusion, and a large area of liquid phase appears, as shown in the white dotted area of Fig. 6d. When t^* =3300, partial remelting also occurs in the non-twinned Grain 1 and Grain 2, as shown in Fig.6d–6e.

The remelted regions of Grain 1 and Grain 2 are small, and the remelted crystallization is completed firstly. During this process, new dislocations are formed, as shown in the yellow dotted regions in Fig.6f–6i. The remelted areas of Grain 3 and Grain 4 are large, and the remelted crystallization process lasts longer. At the last moment of loading, there are still some areas that have not been completely transformed into ordered ones, as shown in the white dotted area of Fig.6i.

Different from the non-twinned grains, a large number of new dislocations will not be generated inside the twinned grains during the remelting and crystallization processes. Besides, a pinned dislocation exists inside the Grain 3, as shown in the yellow dotted areas in Fig. 6f – 6i. Through the thermodynamic phase diagram, it is found that the temperature is very close to the solidus line temperature but does not fall into the solid-liquid two-phase region. However, the material has very obvious remelting and crystallization phenomena, namely overburning phenomenon.

4 Discussion

4.1 Free energy field analysis

It can be seen that the phenomenon of remelting and crystallization will occur when the temperature is too high, which needs to be avoided in the actual production. Therefore, the cases with the temperature coefficient of 0.19 (with remelting and crystallization) and the temperature coefficient of 0.20 (without remelting and crystallization) were further analyzed. Combined with the free energy field and average free energy curve, the influence mechanism of temperature on

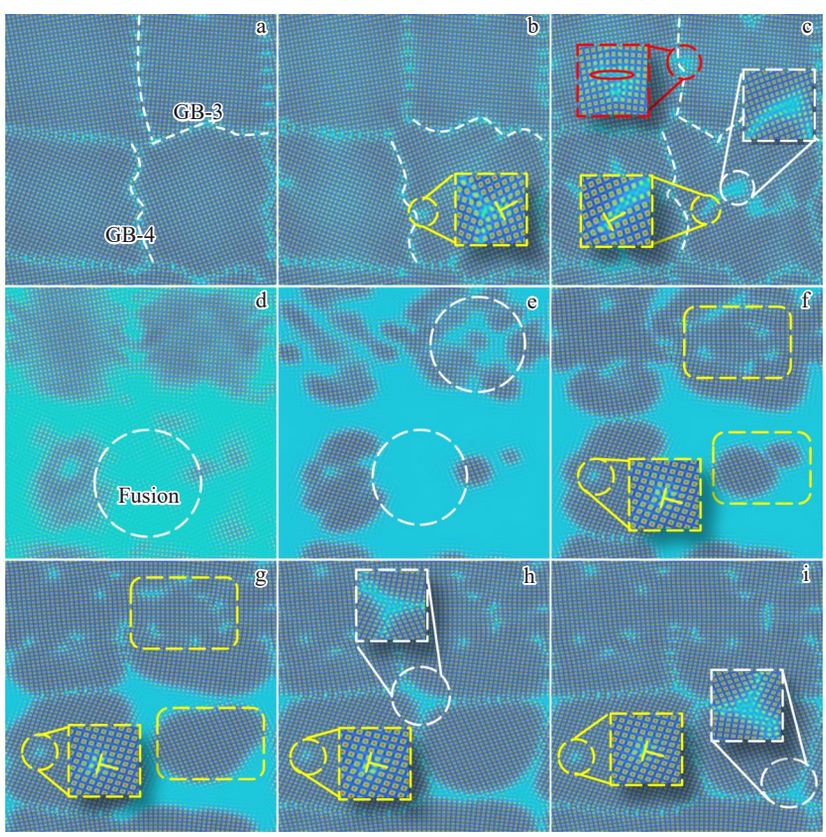

Fig.6 Density field evolution results of multi-directional forging with temperature coefficient ϵ_1=0.19 during one-pass (a), two-passes (b–c), and three-passes (d–i) loading stages: (a) t^*=1500; (b) t^*=2700; (c) t^*=3000; (d) t^*=3100; (e) t^*=3300; (f) t^*=3500; (g) t^*=3700; (h) t^*=3900; (i) t^*=4000

the grain refinement effect of multi-directional forging was discussed.

When the temperature coefficient is 0.19, the free energy field results and the average free energy curve are shown in Fig. 7. During the one-pass loading, GB bending consumes energy, thus reducing the system energy. This stage corresponds to the period before point A in Fig. 7l. At the end of one-pass loading, a large amount of energy is consumed, so GB forms a tip structure. To maintain the existence of the tip, the energy is concentrated at the tip area. Except that, the energy is dispersed on the GB intersection nodes.

When the loading direction changes, the position of energy concentration also changes, so GB deforms along the *y*-axis direction and becomes deformed along the *x*-axis direction. Therefore, the energy for GB parallel to the *x*-axis direction will be transferred to the GB intersection along *x*-axis direction. The direction of energy will be changed from *y*-axis to the direction perpendicular to GB, so GB along *y*-axis direction will be deformed. This process will always consume energy (corresponding to the B-C stage from the average free energy curve in Fig. 7l) until the energy at GB tip exceeds the critical value and is released into the grain interior, as shown in Fig. 7b–7g, therefore increasing the system energy, which corresponds to the C-D stage from the average free energy curve in Fig. 7l. In the three-passes loading stage, the atoms are preferentially transformed from ordered ones into disordered ones at the energy concentration position. This phenomenon will consume a lot of energy and make the free energy of the system decrease rapidly. Then, under the continuous supply of external energy, the crystallization occurs. The liquid phase at the high-energy position in the system will be transformed into a stable crystal structure with more energy. Finally, the energy will be concentrated at the intersection nodes of GB. In this process, the supplied energy is much larger than the energy consumed by the system, so the energy of the system increases, corresponding to the stage

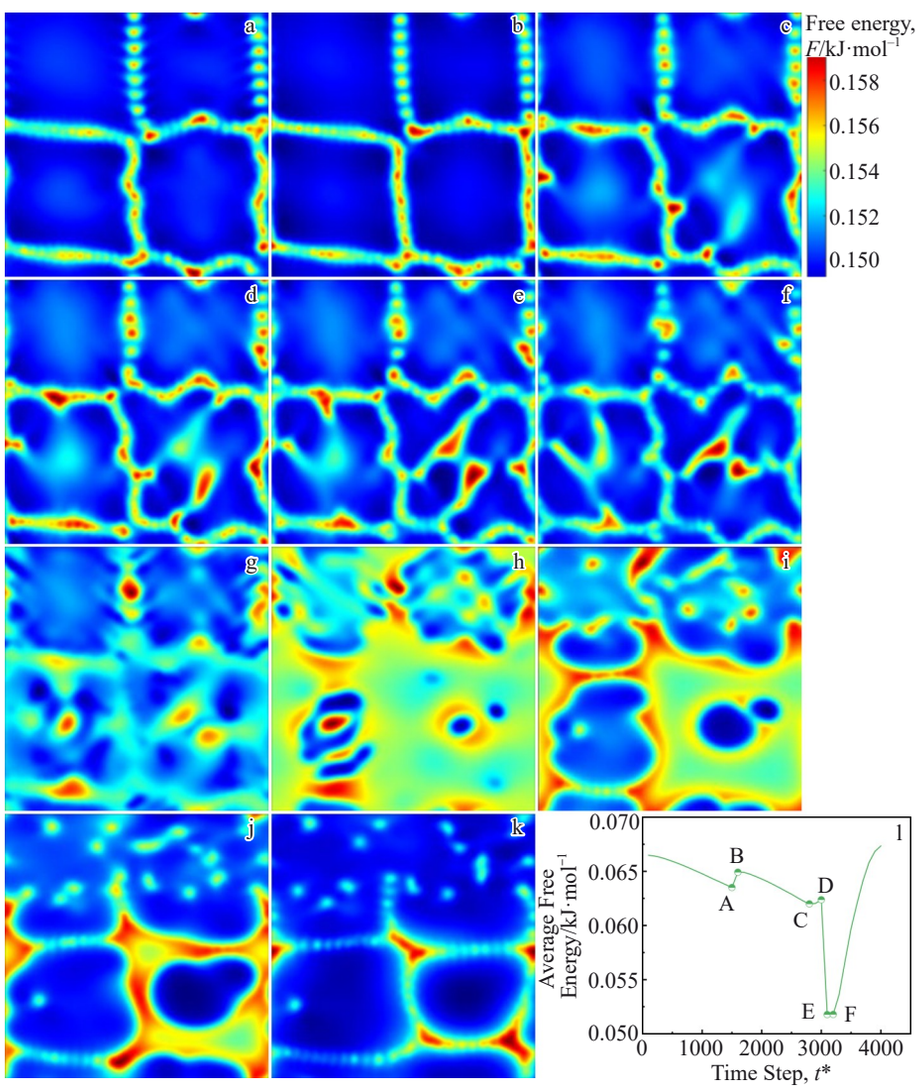

Fig.7 Evolution results of free energy field of multi-directional forging process with temperature coefficient ϵ_1=0.19 during one-pass (a), two-passes (b–f), and three-passes (g–k) loading stages: (a) t*=1500, (b) t*=1600, (c) t*=2700, (d) t*=2800, (e) t*=2900, (f) t*=3000, (g) t*=3100, (h) t*=3200, (i) t*=3500, (j) t*=3700, and (k) t*=4000; average free energy curve of whole process of multi-directional forging with temperature coefficient ϵ_1=0.19 (l)

after the point F on the average free energy curve in Fig.7l.

When the temperature coefficient is 0.20, the free energy field results and the average free energy curve are shown in Fig.8. In the first two loading stages, the energy change trend is similar to that when the temperature coefficient is 0.19. When t^*=2900, the energy at GB tip exceeds the critical value and is released to the grain interior. This phenomenon occurs later, compared with the case with temperature coefficient as 0.19. This result indicates that high temperature will promote the energy release at GB tip to the grain interior. The corresponding atomic density field shows that high temperature will prompt the dislocation at GB tip to move to the grain interior earlier, which conforms to the law of thermodynamics, as shown in Fig.8c–8d.

At the beginning of the three-passes loading, the internal energy of the system is concentrated at GB tip. At a certain time, the energy at GB tip exceeds the critical value and is released to the grain interior, so the system energy will increase. Compared with the case with temperature coefficient as 0.19, there is a small step formed on the free energy curve with temperature coefficient as 0.20 due to the continuous consumption of a large amount of energy caused by pre-melting. At this temperature coefficient, a large amount of energy will be consumed. The absence of any energy-intensive process allows the free energy to continuously increase in this stage, as indicated by the point D in Fig.8l.

4.2 Average free energy curve and refinement result analysis

The average free energy curves of the whole process of multi-directional forging under different temperature conditions are shown in Fig.9. It is found that the average free energies of different schemes are basically the same before the three-passes loading, and they become different since the third pass.

With the increase in temperature coefficient, the free energy consumed in the initial stage of three-passes loading becomes

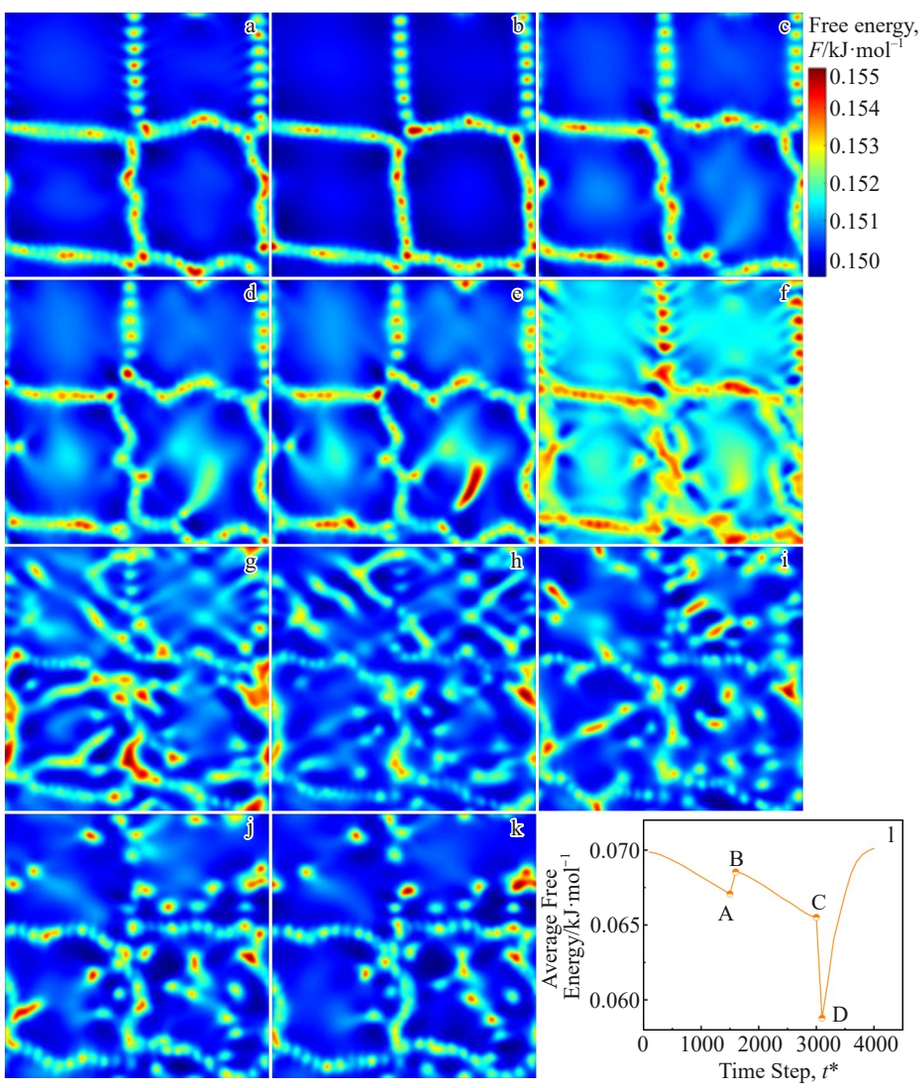

Fig.8 Evolution result of free energy field of multi-directional forging process with temperature coefficient ϵ_1=0.20 during one-pass (a), two-passes (b–e), and three-passes (f–k) loading stages: (a) t^*=1500, (b) t^*=1600, (c) t^*=2600, (d) t^*=2900, (e) t^*=3000, (f) t^*=3100, (g) t^*=3300, (h) t^*=3400, (i) t^*=3600, (j) t^*=3800, and (k) t^*=4000; average free energy curve of whole process of multi-directional forging with temperature coefficient ϵ_1=0.20 (l)

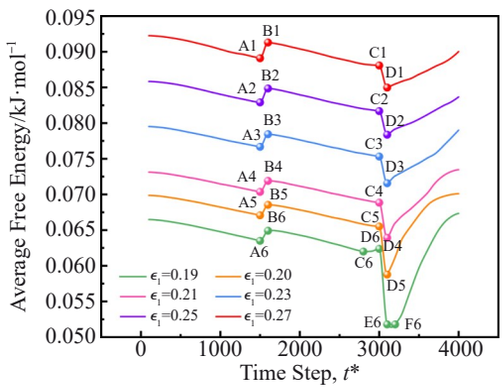

Fig.9 Average free energy curves under different temperature coefficient conditions

more and more, as indicated by the D6-E6 stage with temperature coefficient as 0.19 and the C-D stages with all other temperature coefficient conditions in the average free energy curves. The difference of free energy in these stages is increased with the increase in temperature coefficient. This is because GB will undergo severe deformation at this stage, and atomic dislocation will occur near TB. At the same time, a small number of dislocations from GB will return to TB area under stress. These three phenomena will consume a lot of free energy.

Besides, this stage is related to the moment when the loading direction has just changed. The supplied energy is not enough to offset the energy consumed by the system, so the energy of the initial stage of the three-passes loading decreases sharply. Additionally, as the temperature increases, the intensity of the abovementioned three phenomena will increase, so the system will consume more energy.

When the temperature coefficient is 0.19, the inflection point of the average free energy curve exceeds that under the other five temperature schemes. This phenomenon can be attributed to the three-passes stage. In comparison to the cases with the other five loading temperature coefficients, the result with temperature coefficient of 0.19 allows for a breakthrough at the energy concentration position on GB during the C6-D6 stage within the system. This phenomenon occurs under external stress, resulting in energy release to the grain interior and consequently increasing the overall energy of the system. Thus, there is a slight increase in system energy at this stage.

Subsequently, during the D6-F6 stage, i.e., t^*=3000–3200, a significant remelting phenomenon occurs within the system. Although this process consumes substantial amount of energy, it also leads to the formation of new GB interfaces, which contributes to additional energy. The continuous supply from external condition further facilitates this increase in overall system energy. In contrast, no high-energy-consuming behavior, such as remelting, occurs under any other five loading temperature coefficient conditions. Therefore, there are no processes leading to reformation and subsequent increases in GB interface energies. However, despite this absence of significant internal changes consuming large amount of energy, a consistent supply from external conditions exists, preventing any continuous reduction in total system energy. Hence, under these conditions influenced by external forces, free energy continues to rise.

The number of final grains and the number of dislocations from GB under different temperature coefficients are shown in Fig.10. The number of initial grains before forging is 4. When the temperature coefficients are set as 0.19, 0.20, 0.21, 0.23, 0.25, and 0.27, the numbers of final grains are 9, 13, 15, 32, 30, and 21, respectively. These results indicate that an appropriate temperature coefficient ϵ_1 yields the most significant grain refinement effect. Therefore, in this research, the optimal temperature coefficient is 0.23. In comparison with that at temperature coefficient of 0.19, 0.20, 0.21, 0.25, and 0.27, the refinement effect at temperature coefficient of 0.23 is enhanced by approximately 256%, 146%, 113%, 6.7%, and 52.4%, respectively. The number of dislocations from GB at temperature coefficient of 0.19, 0.20, 0.21, 0.23, 0.25, and 0.27 is 13, 26, 32, 58, 54, and 37, respectively, as shown in Fig. 10b. The change in the number of dislocations corresponds to the grain refinement results. Briefly, when the processing temperature coefficient ϵ_1 is in the range of 0.19 – 0.23, the excessively high temperature provides a considerable driving force for the dislocation movement inside the material, so a large number of dislocations move, eventually encounter with each other, and disappear. However, when the temperature coefficient ϵ_1 is related to the relatively low-temperature range, such as 0.23–0.27, with the increase in temperature, the deformation decomposition and dislocation movement of GBs are promoted, and the total number of dislocations is continuously increased, which leads to the significant effect of dislocation movement on cutting grains,

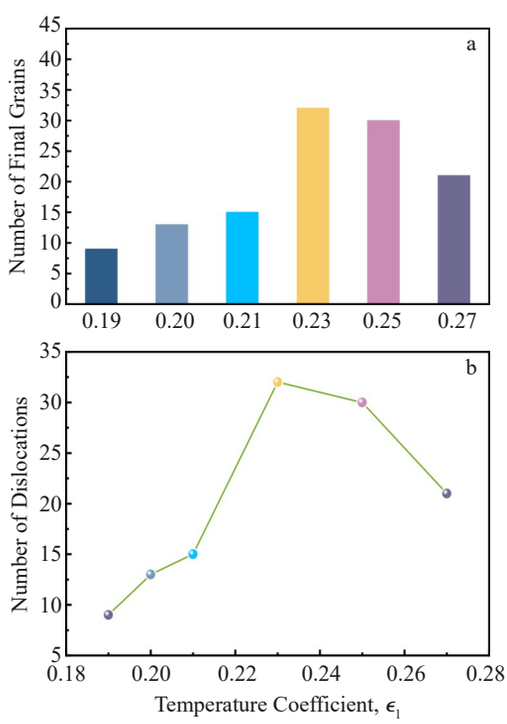

Fig.10 The numbers of final grains (a) and dislocations from GB (b) under different temperature coefficients

and the final grain size becomes smaller.

These findings suggest that excessively high processing temperatures can lead to severe coarsening of grains. Thus, it is imperative to identify the optimal processing temperature during manufacturing to achieve superior material performance.

5 Conclusions

1) The essence of grain refinement and grain coarsening is related to the dislocation movement cutting grains and the high temperature-induced dislocation annihilation and remelting crystallization, respectively. Two nucleation modes of dislocations are revealed: dislocations from GBs and atomic dislocations near TBs. The relevant characteristics provide an atomic-level understanding of the multi-directional forging process.

2) The optimal processing temperature is related to the temperature coefficient ϵ_1 of 0.23. Compared with that at temperature coefficient ϵ_1 of 0.19, 0.20, 0.21, 0.25, and 0.27, the grain refinement effect at ϵ_1=0.23 is increased by 256%, 146%, 113%, 6.7%, and 52.4%, respectively. It is pointed out that when the processing temperature coefficient ϵ_1 is in the range of 0.19–0.23, the excessively high temperature provides a considerable driving force for the dislocation movement inside the material, so a large number of dislocations move, eventually encounter with each other, and disappear. At the same time, the applied strain reduces the melting point of the material, and the processing temperature will still cause remelting, even if it does not exceed the melting point (i. e., overburning phenomenon). Additionally, the crystallization phenomenon may occur. This dynamic process reduces the internal defects of the grains and increases the grain size. However, when the temperature coefficient ϵ_1 falls in the relatively low-temperature range, such as 0.23–0.27, with the increase in temperature, the deformation decomposition and dislocation movement of GBs are promoted, and the total number of dislocations is continuously increased, which leads to the significant effect of dislocation movement on cutting grains, and the final grain size becomes smaller.

References

1 Fu Y F, Huang S Q, Yi Y P *et al*. *Materials & Design*[J], 2024, 239: 112784

2 Liu W, Zhao Y H, Zhang Y T *et al*. *International Journal of Plasticity*[J], 2023, 164: 103573

3 Arjmandabasi T, Révész Á, Kis V K *et al*. *Materials & Design*[J], 2024, 244: 113113

4 Tesař K, Koller M, Vokoun D *et al*. *Materials & Design*[J], 2023, 226: 111678

5 Rao P N, Singh D, Jayaganthan R. *Materials & Design*[J], 2014, 56: 97

6 Zhang Z X, Qu S J, Feng A H *et al*. *Materials Science and Engineering A*[J], 2017, 692: 127

7 Yang Z Y, Liu H W, Cui Z S *et al*. *Materials & Design*[J], 2023, 225: 111508

8 Huang Y J, Wan Y C, Liu C M *et al*. *Journal of Materials Science & Technology*[J], 2024, 181: 41

9 Zhao Y H. *Materials Genome Engineering Advances*[J], 2024, 2(2): e44

10 Zhao Y H, Xin T Z, Tang S *et al*. *MRS Bulletin*[J], 2024, 49(6): 613

11 Boccardo A D, Zou Z, Simonelli M *et al*. *Materials & Design*[J], 2024, 241: 112949

12 Sun Zhipeng, Peng Danmin, Zhang Zikang *et al*. *Rare Metal Materials and Engineering*[J], 2025, 54(7): 1810 (in Chinese)

13 Zhao Y H. *npj Computational Materials*[J], 2023, 9(1): 94

14 Chen W P, Hou H, Zhang Y T *et al*. *Acta Metallurgica Sinica* (*English Letters*)[J], 2023, 36(11): 1791

15 Yang W K, Wang K L, Pei J Q *et al*. *Computational Materials Science*[J], 2023, 228: 112338

16 Chen L Q, Zhao Y H. *Progress in Materials Science*[J], 2022, 124: 100868

17 Xin T Z, Zhao Y H, Mahjoub R *et al*. *Science Advances*[J], 2021, 7(23): eabf3039

18 Pei Jiaqi, Hou Hua, Yang Wenkui *et al*. *Rare Metal Materials and Engineering*[J], 2024, 53(3): 834 (in Chinese)

19 Zhao Y H, Xing H, Zhang L J *et al*. *Acta Metallurgica Sinica* (*English Letters*)[J], 2023, 36(11): 1749

20 Xu B, Sun Y Z, Yu C *et al*. *International Journal of Plasticity*[J], 2024, 177: 103993

21 Liang X, Bos C, Hermans M *et al*. *Materials & Design*[J], 2023, 235: 112424

22 Sun Qiming, Shen Wenlong, Liao Yuxuan *et al*. *Rare Metal Materials and Engineering*[J], 2025, 54(3): 671 (in Chinese)

23 Zhu Wei, Cheng Dazhao, Liu Caiyan *et al*. *Rare Metal Materials and Engineering*[J], 2024, 53(8): 2193 (in Chinese)

24 Cui Shushan, Shi Tao, Lu Chao *et al*. *Rare Metal Materials and Engineering*[J], 2023, 52(10): 3374 (in Chinese)

25 Pei X L, Pei J Q, Hou H *et al*. *npj Computational Materials*[J], 2025, 11(1): 27

26 Elder K R, Katakowski M, Haataja M *et al*. *Physical Review Letters*[J], 2002, 88(24): 245701

27 Guo C, Wang J C, Li J J *et al*. *Acta Materialia*[J], 2018, 145: 175

28 Li L M, Li H Q, Lei P Y *et al*. *Journal of Magnesium and Alloys*[J], 2025, 13(2): 697

29 Xin T Z, Tang S, Ji F *et al*. *Acta Materialia*[J], 2022, 239: 118248

30 Shuai C, Liu W Q, Li H W *et al*. *International Journal of Plasticity*[J], 2023, 170: 103772

31 Li M X, Li H Q, Liu Y H *et al*. *Materials Science and Engineering A*[J], 2023, 884: 145562

32 Tian X L, Zhao Y H, Peng D W *et al*. *Transactions of Nonferrous Metals Society of China*[J], 2021, 31(4): 1175

33 Xu X T, Song Z, Wang K L *et al*. *Journal of Materials Science & Technology*[J], 2025, 219: 307

34 Guo Q W, Hou H, Wang K L *et al*. *npj Computational Materials*[J], 2023, 9(1): 185
35 Blixt K H, Hallberg H. *Materials & Design*[J], 2022, 220: 110845
36 Zhang S X, Wu L, Gu T *et al*. *Journal of Alloys and Compounds*[J], 2022, 923: 166413
37 Song X Q, Wang Y X, Zhang J *et al*. *Materials Science and Engineering A*[J], 2021, 806: 140820
38 Tian X L, Zhao Y H, Gu T *et al*. *Materials Science and Engineering A*[J], 2022, 849: 143485
39 Li H Q, Zhao Y H, Song Z *et al*. *Acta Materialia*[J], 2025, 301: 121573
40 Song Z, Li H Q, Wang X N *et al*. *Journal of Materials Research and Technology*[J], 2023, 27: 6501

多向锻造工艺最优温度设计：晶体相场研究

宋　卓[1]，李欢庆[1]，田晓林[1]，康晓兰[1]，侯　华[1,4]，赵宇宏[1,2,3]
(1. 中北大学 材料科学与工程学院 教育部山西省共建铝/镁材料研发应用协同创新中心
新材料智能铸造先进成型山西省重点实验室，山西 太原 030051)
(2. 北京科技大学 北京材料基因工程高精尖创新中心，北京 100083)
(3. 辽宁材料实验室 材料智能技术研究所，辽宁 沈阳 110004)
(4. 太原科技大学 材料科学与工程学院，山西 太原 030024)

摘　要：以多向锻造温度为自变量，采用双模晶体相场模型，研究了不同温度下的形核模式、反应机制及晶界-位错相互作用。结果表明：建立了工艺参数与晶粒细化/粗化的映射关系，确定最优加工温度系数为0.23。相较于0.19、0.20、0.21、0.25及0.27等加工温度系数条件下，细化效果分别提升256.0%、146.0%、113.0%、6.7%和52.4%。温度过高会因位错湮灭导致晶粒粗化；施加应变会降低材料实际熔点。即使加工温度未超过理论熔点，仍可能发生熔化与重结晶，引发过烧现象——该现象在减少内部缺陷的同时会导致晶粒整体粗化。本研究对实际锻造工艺设计具有重要指导意义。

关键词：晶体相场法；多向锻造；温度；晶粒细化；位错

作者简介：宋 卓，男，1998年生，博士生，中北大学材料科学与工程学院教育部山西省共建铝/镁材料研发应用协同创新中心新材料智能铸造先进成型山西省重点实验室，山西 太原 030051，E-mail：B20240313@st.nuc.edu.cn